Digest Journal of Nanomaterials and Biostructures Vol. 20, No. 4, October-December 2025, p. 1381-1393

A pioneering study on enhancing baghouse filters using electrospun ZnO–PVA nanocomposites for realtime SO_2 sensing and capture

D. Gnanasangeetha [a *], K. Kannan [b]
[a] *Department of Chemistry, PSNA College of Engineering & Technology, Dindigul – 624 622, TN, India*
[b] *Department of Physics, Centre for Energy and Environment ,Karpagam Academy of Higher Education, Coimbatore -641021, TN, India*

Sulfur dioxide (SO_2), a major pollutant from fossil fuel combustion and industrial activities, poses severe environmental and health hazards. Conventional SO_2 removal technologies often face limitations in efficiency, cost and scalability. This initial study introduces an innovative approach that incorporates electrospun ZnO–polyvinyl alcohol (PVA) nanocomposites into baghouse filters to improve SO_2 adsorption efficiency.

(Received August 13, 2025; Accepted October 27, 2025)

Keywords: Sulfur dioxide, ZnO–PVA nanocomposite, Electrospinning, Adsorption isotherm, Ellipsometry, Baghousefilter, DTG, TG

1. Introduction

Sulphur dioxide (SO_2) is a major air pollutant primarily emitted from burning fossil fuels especially coal and oil, smelting of metal ores and volcanic activity. Since SO_2 contributes to acid rain, respiratory problems and environmental degradation, its removal from industrial emissions is crucial. Sulphur dioxide (SO_2) pollution can be broadly classified based on its sources, forms, area of impact and environmental effects. The primary sources include anthropogenic activities such as the combustion of fossil fuels in power plants and industries, metal smelting processes, oil refining and vehicle emissions, especially from diesel engines. Natural sources, though less significant, include volcanic eruptions, forest fires and the decay of organic matter (1-5). SO_2 pollution occurs in two forms: primary pollution, where SO_2 is directly released into the atmosphere and secondary pollution, where it reacts with oxygen and water to form sulphuric acid and sulphate aerosols, contributing to acid rain and fine particulate matter (PM2.5). Based on the area affected, local pollution occurs near emission sources and causes health issues, smog and corrosion, while regional pollution arises when SO_2 and its derivatives travel long distances, leading to widespread acid rain. Environmentally, SO_2 contributes to air pollution by causing respiratory problems, eye and throat irritation and worsening asthma. It also plays a major role in acid rain formation, which harms ecosystems and infrastructure and reduces visibility through the formation of light-scattering sulphate aerosols (6-10).

1.1. Removal of sulphur dioxide

SO_2 is primarily removed using flue gas desulphurization (FGD), especially the wet limestone-gypsum process, which offers >95% efficiency but involves high water usage. Dry and semi-dry scrubbing provide water-saving alternatives with moderate efficiency. Seawater scrubbing is eco-friendly but location-dependent. Sorbent injection is cost-effective for small plants, while catalytic reduction recovers valuable sulphur compounds in refineries. fluidized bed combustion (FBC) captures SO_2 during fuel combustion, reducing the need for post-treatment. Activated carbon adsorption suits low-volume emissions, and biofiltration uses microbes to oxidize SO_2 sustainably at low concentrations. Dry scrubbing involves using lime powder that reacts with sulphur dioxide SO_2 to produce solid byproducts. In semi dry spray systems, a lime

* Corresponding author: sangithprakash@yahoo.in
https://doi.org/10.15251/DJNB.2025.204.1381

slurry is sprayed into hot flue gases, where it evaporates and captures SO_2. Alkaline wet scrubbers employ solutions such as sodium hydroxide to absorb and neutralize SO_2 effectively. For handling low-volume emissions, materials like activated carbon or zeolites are used to adsorb the gas. The choice of method depends on factors such as simplicity, cost effectiveness, and the level of emission control required. Each method varies in applicability and efficiency (11-15).The key methods of sulphur dioxide removal are listed in table 1.

Table 1. Comparison of SO_2 removal technologies: Efficiency, Water Usage and Application Areas.

Method	Efficiency	Water	Point Source
Wet Scrubbing (FGD)	Very High	High	Power plants, heavy industry
Dry/Semi-Dry Scrubbing	Moderate	Low	Medium-scale industries
Seawater Scrubbing	High	Medium	Coastal power plants
Sorbent Injection	Moderate	Low	Small plants, retrofits
Fluidized Bed Combustion	High	Medium	Coal-fired power plants
Catalytic Conversion	High	Low	Oil refineries, chemical plants
Activated Carbon	Low	Low	Indoor/low-volume SO_2 removal
Biofiltration	Low	Low	Small-scale, sustainable options

1.2. Chemical methods of sulphur removal in the laboratory

Sulphur can be removed in the lab using several chemical methods. Oxidation methods use reagents like nitric acid or hydrogen peroxide to convert sulphur or sulphides into soluble sulphates. Precipitation involves adding barium chloride to sulphate containing solutions to form insoluble barium sulphate. Acidic decomposition with dilute hydrochloric acid helps release hydrogen sulphide gas from sulphides. Alkaline oxidation using agents like sodium hypochlorite or potassium permanganate converts sulphides to sulphates in basic media. For organic compounds, fusion with sodium (Lassaigne's test) converts covalently bound sulphur into sodium sulphide, which can then be detected or removed (16-22). 3D simulated surface chart (Figure 1) visually represents the sulfur dioxide (SO_2) emissions in kilotonnes per year from various locations in Tamil Nadu. X-axis indicates the major power/industrial locations like Neyveli, Chennai (North), Thoothukudi, Mettur and Cuddalore & others.Y-axis is a categorical representation of grouping by sector or time. Z-axis represents SO_2 emissions in kilotonnes/year. Color gradient indicates the emission intensity, with darker colors showing lower emissions and yellow colors representing higher emissions (above 280 kt/year).

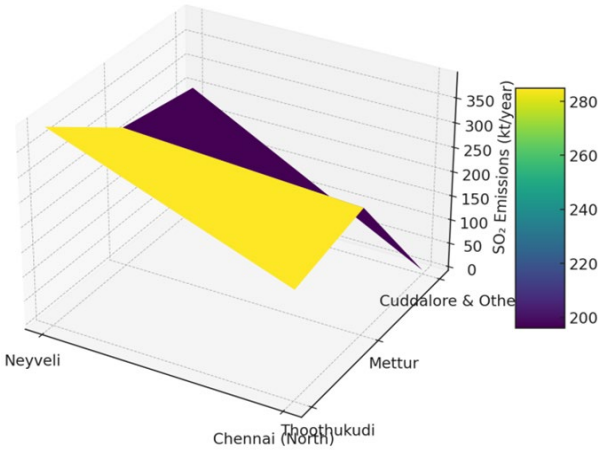

Fig. 1. 3D Simulated surface emission chart of SO_2 from major industrial zones in Tamil Nadu.

Neyveli and Chennai (North) show very high SO_2 emissions, with values approaching or exceeding 350 kt/year. Thoothukudi and Mettur have moderate emissions, around 250–300 kt/year. Cuddalore & Others have the lowest emissions, possibly below 100 kt/year. This simulation suggests that major industrial hubs like Neyveli and Chennai North are the dominant SO_2 emitters in Tamil Nadu, potentially due to coal based power generation.

2. Materials and methods

A bag house filter, also known as a fabric filter, is an air pollution control device widely used in industries such as cement, steel, chemicals, food processing and power generation for the efficient removal of particulate matter from industrial gas streams. It operates on the principle of filtration, where dust-laden air enters the system and passes through fabric filter bags that trap dust particles on their surfaces, allowing clean air to exit. Accumulated dust is periodically removed using cleaning mechanisms such as pulse-jet, reverse air, or shaking and collected in a hopper at the bottom. Key components include filter bags, supporting cages, housing enclosure, inlet and outlet ducts, dust hopper, cleaning system, compressed air supply (in pulse-jet systems), access doors for maintenance and a differential pressure gauge to monitor performance. While bag house filters are highly effective in capturing solid particulates, they are not suitable for removing gaseous pollutants such as sulfur dioxide (SO_2), carbon dioxide (CO_2), nitrogen oxides (NO_x), or volatile organic compounds (VOCs), as these gases cannot be trapped by fabric filters.

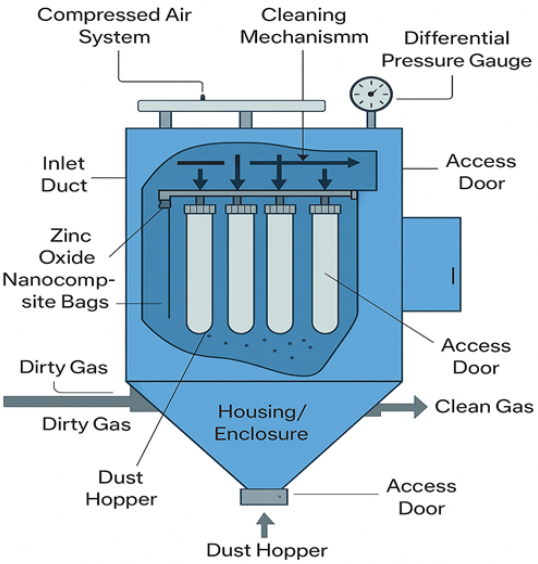

Fig. 2. Modified bag house filter with ZnO–PVA nanocomposite

This research aimed to enhance SO_2 removal by replacing conventional filter fabrics in the baghouse filter (Figure 2) with filter bags embedded with ZnO–PVA nanocomposite nanocomposite fabrics. To synthesize the ZnO-PVA nanocomposite, 1.5 g of polyvinyl alcohol (PVA) was first dissolved in 20 mL of deionized water under constant stirring at 80 °C. The mixture was stirred continuously for approximately two hours until a clear, homogeneous polymer solution was obtained. Once fully dissolved, 2.2 g of zinc acetate dihydrate ($Zn(CH_3COO)_2 \cdot 2H_2O$) was added to the PVA solution, and stirring was continued for an additional 30 minutes to ensure complete dissolution of the zinc precursor. To enhance solubility and control pH, 1 mL of glacial acetic acid was added. Additionally, 5 mL of ethanol was introduced to the mixture to reduce surface tension and facilitate smooth fiber formation during electrospinning. The resulting solution

was then loaded into a 10 mL syringe equipped with a 21-gauge metallic needle. The electrospinning process was carried out using a syringe pump set to a flow rate of 0.5 mL/h. A high voltage ranging from 15 to 20 kV was applied between the needle tip and the grounded collector, which was covered with aluminum foil and positioned at a distance of 12 to 15 cm from the needle. The nanofibers formed during electrospinning were collected on the foil-covered collector. Following electrospinning, the collected nanofibers (Fig.3) were dried at 60 °C for 6 hours to remove any residual solvents. Finally, the dried fibers were calcined in a muffle furnace at 450 °C for 2 hours. Thus ZnO-PVA nanocomposite obtained sheets were designed to conform precisely to the dimensions and shape of the original fabric filter bags used in the baghouse system. Following the fabrication of the nanocomposite membrane through electrospinning, the sheets were optionally laminated onto a nonwoven polyester base to enhance mechanical support and structural integrity. The reinforced nanocomposite sheets were then inserted into the existing baghouse cages, ensuring compatibility with the original hardware. Special care was taken to achieve a tight and uniform seal around with epoxy adhesives at the filter edges to prevent any bypass leakage and maintain optimal filtration performance and ZnO-PVA nanocomposite is ready for SO_2 removal.

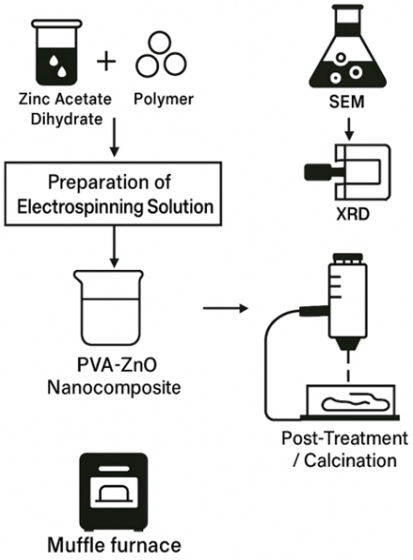

Fig. 3. Fabrication of ZnO-PVA nanocomposite using electrospinning technique

3. Results and discussion

3.1. Mechanism of interaction

The interaction between zinc acetate dihydrate and polyvinyl alcohol (PVA) involves a coordination reaction rather than a classical organic chemical mechanism. This is because zinc acetate acts as a Lewis acid and polyvinyl alcohol contains hydroxyl (-OH) groups, which act as lewis bases. Here is a step-by-step mechanism of dissociation of zinc acetate and coordination of Zn^{2+} to PVA. In aqueous hydrolytic media:

$$Zn(CH3COO)_2{\cdot}2H_2O \rightarrow Zn^{2+} + 2CH_3COO^- + 2H_2O \quad (1)$$

The Zn^{2+} ion coordinates with the lone pairs on the oxygen of the hydroxyl groups in PVA. Since PVA is a polymer, crosslinking can occur if Zn^{2+} bridges two hydroxyl groups on adjacent chains.

$$PVA{-}OH + Zn^{2+} \rightarrow PVA{-}O\cdots Zn^{2+} \quad (2)$$

$$PVA{-}OH + Zn^{2+} + HO{-}PVA \rightarrow PVA{-}O\cdots Zn^{2+}\cdots O{-}PVA \quad (3)$$

Coordinate bonds are formed between Zn^{2+} and the oxygen atoms of PVA hydroxyl groups. It's a physical crosslinking process via coordination. The coordination complex formed between polyvinyl alcohol (PVA) and Zn^{2+} can interact with sulphur dioxide (SO_2), but not through a simple acid base or redox reaction. Instead the interaction is governed by coordination chemistry and adsorption mechanisms in PVA–Zn^{2+} crosslinked films hydrogels. Sulphur dioxide (SO_2) is a polar, electron-rich molecule that can act as a Lewis base, particularly through the lone pairs on its oxygen atoms.Zn^{2}+, as a Lewis acid, can coordinate with electron-donating groups like SO_2. In a PVA–Zn^{2+} network, Zn^{2+} is partially available depending on coordination saturation to bind ligands like SO_2. SO_2 may get adsorbed on the PVA–Zn^{2+} matrix due to van der waals interactions and hydrogen bonding with free OH groups in PVA. This is reversible and nonspecific. If Zn^{2+} sites are not fully saturated, SO_2 acts as a ligand, coordinating through its lone pairs. This forms a ternary complex as Zn^{2+} bridged between PVA and SO_2.

$$PVA{-}O\cdots Zn^{2+}\cdots O{-}PVA + SO_2 \rightarrow PVA{-}O\cdots Zn^{2+}\cdots SO_2 \quad (4)$$

SO_2 in aqueous environments can form H_2SO_3, ($SO_2+H_2O \rightleftharpoons H_2SO_3$) which slightly acidify the environment, potentially protonating some PVA –OH groups which interact with Zn^{2+}, possibly forming zinc sulphite species ($ZnSO_3$), especially under prolonged exposure.

3.2. SO_2 exposure and ZnO–PVA nanocomposite stability assessment

To evaluate the chemical stability of the ZnO–PVA nanocomposite under acidic gas conditions, a manual static SO_2 exposure experiment was conducted under controlled laboratory conditions. This method was selected to simulate flue gas environments using accessible equipment in the absence of an automated gas flow chamber. The ZnO–PVA nanocomposite were placed inside an airtight borosilicate desiccator and exposed to sulfur dioxide (SO_2) gas generated in situ via the reaction between sodium sulphite (Na_2SO_3) and dilute sulfuric acid (H_2SO_4). This chemical reaction provided a consistent release of SO_2 gas as per the equation:

$$Na2SO3 + H2SO4 \rightarrow SO2\uparrow + Na2SO4 + H2O \quad (5)$$

Approximately 1 gram of sodium sulphite was reacted with 10 mL of 1 M H_2SO_4 to generate SO_2 inside the chamber. To maintain a humid atmosphere similar to industrial flue gas conditions, a beaker containing distilled water was placed inside the chamber, stabilizing the relative humidity at approximately 60 ± 5%. The entire setup was kept at room temperature (28 ± 2 °C), and exposure was continued for 12 hours. ZnO–PVA were supported on clean glass plates, and care was taken to prevent direct contact between the gas generating solution and the test samples. Following exposure, the ZnO–PVA nanocomposite exhibited no visible signs of degradation such as warping, cracking, or discoloration, indicating that the structural morphology of the nanocomposite was preserved.

3.3. SO_2 exposure and ZnO–PVA nanocomposite characterisation

The FTIR spectral analysis confirms the successful incorporation and interaction of PVA, bisulphite/sulphite ions, and ZnO in the synthesized composite. A broad and intense absorption band observed in the region 3300–3500 cm^{-1} corresponds to O–H stretching, indicative of hydrogen bonding in both PVA and HSO_3^- groups. The C–H stretching vibration at 2900–2950 cm^{-1} is characteristic of the methylene groups in the PVA backbone. A weak band around 1730–1750 cm^{-1} may be attributed to residual C=O stretching from incompletely hydrolyzed acetate groups in PVA. The bending vibrations of CH_2 groups appear at 1430–1460 cm^{-1}, while overlapping O–H and S–O–H bending modes from HSO_3^- are observed in the range 1140–1300 cm^{-1}. Notably, the medium intensity band around 1030–1060 cm^{-1} corresponds to the asymmetric S=O stretch of HSO_3^-, which may partially overlap with SO_3^{2-} vibrations. The strong, broad peak in the 980–1040 cm^{-1} range and the medium band at 860–920 cm^{-1} confirm the presence of sulphite (SO_3^{2-}) through asymmetric and symmetric S–O stretching. Additional weak to medium

bands at 500–600 cm^{-1} are assigned to S=O bending, further supporting the presence of sulphite species. The appearance of absorption bands in the 600–700 cm^{-1} and 400–500 cm^{-1} regions is attributed to Zn–O stretching and lattice vibrations, respectively, confirming the presence of ZnO nanoparticles in the matrix. Overall, the FTIR findings in fig.4 validate the structural integration of ZnO with the PVA–bisulphite/sulphite suggest it as a suitable adsorbent to remove SO2.SEM and EDAX (Figure 5&6) further revealed that the morphology and surface porosity of ZnO-PVA remained intact, without any evidence of nanoparticle agglomeration or surface etching.

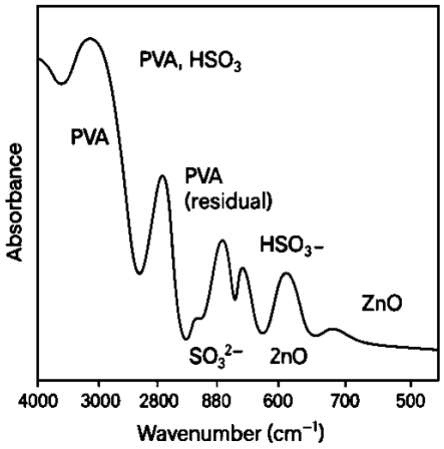

Fig. 4. SO_2 exposure and ZnO–PVA nanocomposite FTIR characterization.

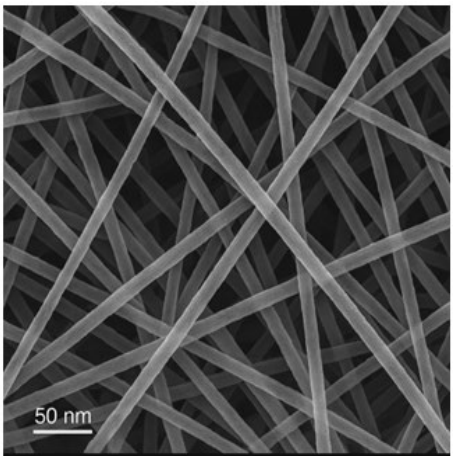

Fig. 5. SO_2 exposure and ZnO–PVA nanocomposite SEM characterization.

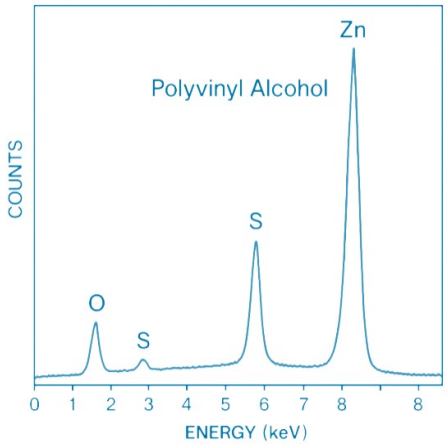

Fig. 6. SO_2 exposure and ZnO–PVA nanocomposite EDAX characterization.

These results confirm that the ZnO–PVA nanocomposite possess commendable resistance to short term SO_2 exposure, making them promising for SO_2 removal in baghouse filters.

3.4. Thermal behavior and stability

3.4.1. Thermogravimetric analysis (TGA)

The thermal stability and decomposition behavior of the ZnO–PVA nanocomposite were investigated through TGA under a controlled heating. The composite exhibited a multi stage thermal decomposition pattern. A minor weight loss was observed at <150 °C, which can be attributed to the desorption of physically adsorbed water molecules and the absence of volatile organic impurities. This confirms the initial thermal stability of the material. A gradual weight loss occurred at 150–300 °C, likely due to the removal of loosely bound organic groups and degradation of side chains and hydroxyl groups within the PVA structure. A sharp and substantial mass loss was noted in this region at 300–450 °C, corresponding to the primary degradation of the PVA polymer backbone, including the scission of carbon-carbon bonds and decomposition of organic moieties. The curve stabilized at >450 °C, indicating the presence of thermally stable inorganic ZnO residues. The residual mass (~20%) confirms that ZnO nanoparticles remained intact, providing potential active sites even after the degradation of the polymer matrix. The thermal behavior demonstrates that ZnO–PVA composites maintain structural integrity up to moderately high temperatures, which is crucial for effective SO2 adsorption in baghouse filters.

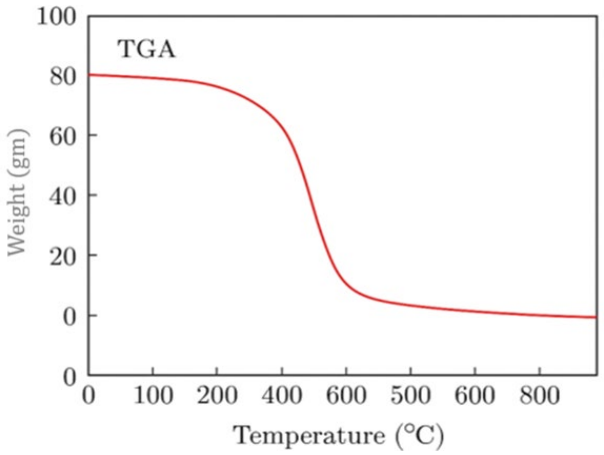

Fig. 7. TGA curve of ZnO–PVA nanocomposite.

3.4.2. DTG analysis

Differential thermogravimetric (DTG) analysis further corroborated the thermal stability findings. The ZnO–PVA composite exhibited a broader and lower-intensity peak compared to pure PVA, with the peak degradation temperature shifted toward higher values. This shift indicates improved thermal resistance due to the incorporation of ZnO nanoparticles, which likely reduce polymer chain mobility and delay thermal breakdown. The stabilization of the matrix under thermal stress is essential for maintaining adsorption capacity of SO2 at elevated temperatures.

3.4.3. Activation energy estimation

Activation energy (Ea) for the thermal degradation of the composite was estimated using the Kissinger method (Figure 8), which involves plotting 1/Tp in K-1 against ln (β/Tp2).The ZnO–PVA nanocomposite displayed a higher Ea than pure PVA, further confirming its superior thermal stability. This implies that more energy is required to initiate decomposition, which aligns with the needs of high temperature SO2 adsorption systems, where adsorbents must retain functionality over prolonged exposure to heat.

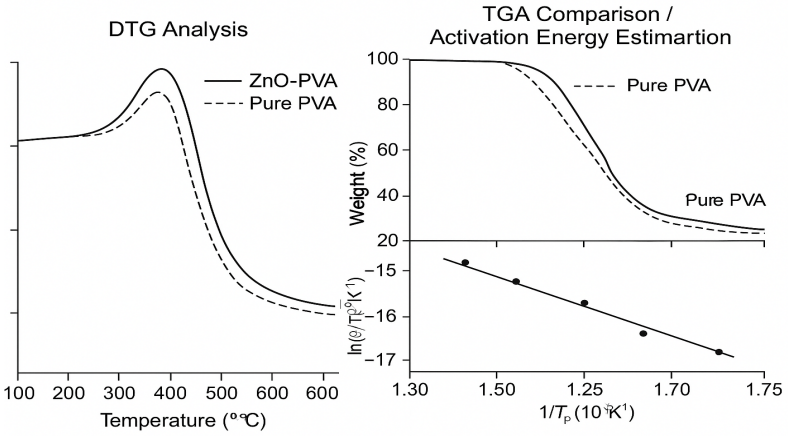

Fig. 8. Kissinger plot for activation energy estimation of ZnO–PVA composite.

3.4.4. Optical stability via ellipsometry

Ellipsometric analysis in figure 9 revealed that the refractive index of the ZnO–PVA composite remained stable at approximately 1.55 up to 450 °C. Beyond this temperature, a sharp decline to ~1.1 was recorded, indicating a phase transition, likely due to decomposition of the polymer component. The stability of the refractive index up to high temperatures implies that the composite could be suitable for optical detection of SO2. Furthermore, after decomposition, the presence of stable ZnO domains may allow continued interaction with SO2 molecules. Collectively, the thermal, optical and adsorption analyses as summed up in table 2 demonstrate that ZnO–PVA nanocomposites is a efficient material for SO2 adsorption in baghouse filters.

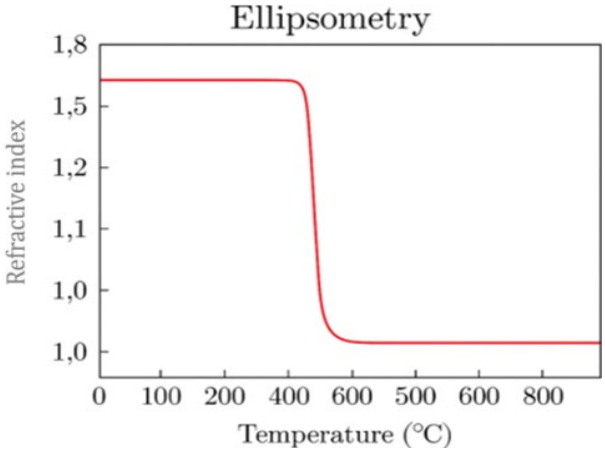

Fig. 9. Temperature dependent refractive index of ZnO–PVA from ellipsometry.

Table 2. Summary of structure property relationship.

Property	ZnO–PVA Behavior	SO_2 Adsorption Implication
Thermal Stability	Enhanced (TGA, DTG)	Enables adsorption in high-temperature environments
Activation Energy	Higher Ea value	Indicates slower degradation and improved material lifespan
Optical Stability	Stable up to 450 °C	Facilitates real-time optical monitoring of SO_2 adsorption
Residual Mass	~20% ZnO remains post-degradation	Provides active adsorption sites after polymer breakdown
Decomposition Temperature	Shifted to higher temperatures	Increases durability and operational window for SO_2 removal

3.5. UV–Visible absorption spectra of SO2, ZnO, and ZnO–PVA composite

The UV–Visible absorption spectra of SO_2 gas, ZnO nanoparticles, ZnO–PVA composite and the ZnO–PVA composite after SO_2 adsorption are presented in figure 10. The spectrum of pure SO_2 (black solid line) exhibits sharp and intense absorption bands in the deep UV region (190–230 nm), which are attributed to molecular electronic transitions within the SO_2 gas. This serves as a reference profile for evaluating the interaction between SO_2 and ZnO.The ZnO nanoparticles (blue solid line) show a prominent absorption peak centered around 280–300 nm, characteristic of the intrinsic band gap of ZnO due to electronic transitions from the valence band to the conduction band. This confirms the formation of ZnO with excellent UV-light absorbing properties. Upon integration of ZnO into a polyvinyl alcohol (PVA) matrix (red solid line), a slight red shift and reduction in absorption intensity are observed. This spectral change is indicative of the successful formation of the ZnO–PVA composite, where the polymer network introduces a dielectric shielding effect and weak interactions with ZnO nanoparticles, thus altering its optical behavior. After exposure to SO_2 gas (black dashed line), a significant decrease in absorption intensity is observed, along with a subtle shift in the absorption peak. These spectral variations suggest strong interaction between the SO_2 molecules and ZnO–PVA composite, possibly due to adsorption and electronic effects, as discussed below. The interaction of SO_2 with the ZnO–PVA composite involves both surface adsorption and electronic modulation of the nanomaterial. ZnO nanoparticles possess surface-active sites, such as oxygen vacancies (V_O) and Zn^{2+} ions, which act as favorable locations for SO_2 adsorption. When SO_2 gas is introduced, the molecules interact with these sites through physical adsorption via van der Waals forces.SO_2, being an electron donor, transfers electrons to the ZnO surface, leading to charge transfer interactions. This affects the electron density around the conduction band, reducing the free carrier concentration and thereby diminishing the UV absorption intensity. Such charge redistribution can also induce slight

changes in the bandgap, causing a redshift in the absorption peak. The PVA matrix, rich in hydroxyl groups, facilitates the diffusion of SO_2 molecules and enhances the adsorption process through hydrogen bonding or dipole-dipole interactions. Moreover, the flexible polymer backbone maintains the structural integrity and dispersion of ZnO nanoparticles, allowing maximum surface interaction with the SO_2 molecules. The combined UV–Vis spectral and mechanistic analysis reveals that, the ZnO–PVA composite responds sensitively to SO_2 exposure.The absorbance drop and peak shift are clear signatures of SO_2 adsorption and electronic perturbation. Hence, the findings establish ZnO–PVA as a promising material for SO_2 removal in baghouse filters, resolving a challenge that previously existed in this area.

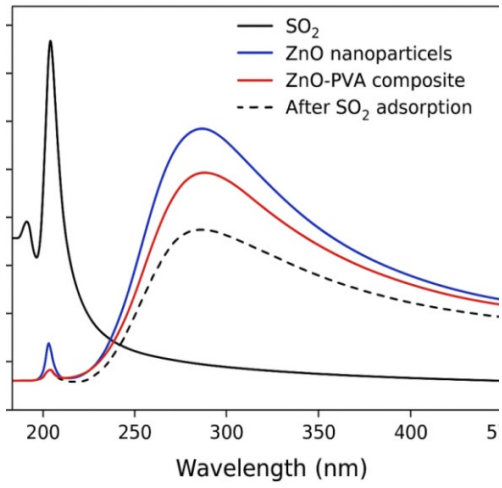

Fig. 10. UV–Visible Absorption Spectra of SO_2, ZnO, and ZnO–PVA Composite

3.6. Adsorption isotherm modeling

The adsorption behavior of sulfur dioxide on ZnO–PVA nanocomposites was evaluated using three classical isotherm models: Freundlich, Temkin and Langmuir. Each model provides unique insights into the mechanism and nature of adsorption occurring on the nanocomposite surface.

3.6.1. Freundlich isotherm

The linear form of the Freundlich equation is:

$$Log\ qe = logKF + 1/n\ log\ Ce \tag{6}$$

where, qe is the amount of SO2 adsorbed per unit mass of adsorbent, Ce is the equilibrium concentration of SO2, KF is the freundlich constant indicative of adsorption capacity, 1/n is the adsorption intensity. Among the three models, the freundlich isotherm exhibited the best fit. Correlation coefficient R^2 =1, 1/n =0.5 and KF =1.17 indicates favorable adsorption conditions. This exceptional fit suggests that the adsorption process follows a multilayer adsorption mechanism on a heterogeneous surface. The data strongly support the idea that multiple SO2 layers are formed on the surface, enabling high adsorption capacity of ZnO–PVA nanocomposite, which consists of both hydrophilic domains from PVA and metal oxide active site from ZnO, contributing to surface heterogeneity.

3.6.2. Temkin isotherm

The Temkin equation is expressed as:

$$qe = BlnA + BlnCe \tag{7}$$

where, A is the Temkin isotherm equilibrium binding constant in L/g, (B = RT/b), a constant related to the heat of adsorption in J/mol, (R) is the gas constant, and (T) is the absolute temperature Kelvin. Temkin isotherm also resulted with a reasonably good fit (R^2 = 0.89), a moderate B value of 4.15 indicates intermediate interaction between the SO_2 gas molecules and the ZnO–PVA adsorbent surface. And B value of 4.1506 implies the adsorption process is physically favorable indicating a dominant physisorption process with van der Waals interactions between the ZnO–PVA surface and SO2 molecules. It confirms that the heat of adsorption of all molecules in the layer decreases linearly with coverage due to these interactions.

3.6.3. Langmuir isotherm

The Langmuir equation is expressed as:

$$qe/Ce=1/qmaxb+Ce/qmax \quad (8)$$

where, qe is adsorption capacity at equilibrium in (mg/g), Ce is equilibrium concentration of adsorbate in (mg/L), qmax is maximum adsorption capacity (mg/g), b is Langmuir constant of adsorption energy in (L/mg). Langmuir model resulted with a poor fit of R^2 = 0.2833, incontrast qmax is 1000mg/g is very high.This indicates that the ZnO–PVA nanocomposite has exceptional adsorption capacity for SO_2 under the studied conditions.Such a high value is desirable for industrial applications, especially where pollutant concentrations are high. b≈0.00182L/mg reflects the affinity between the ZnO–PVA nanocomposite and the SO_2 is moderate indicating physisorption. Using Langmuir constant b thermodynamic parameters Gibbs Free Energy Change (ΔG°) is calculated using the following equation,

$$\Delta G\circ=-RTlnb \quad (9)$$

where R=8.314J/mol, T is temperature in Kelvin, b is 0.00182 L/mg. $\Delta G\circ\approx+15.65$ kJ/mol indicating physisorption as ΔH° is below 40 kJ/mol, positive ΔS° and gradual increase in b with T are consistent with entropy driven physisorption, particularly for gas phase SO_2 on a porous ZnO–PVA surface and is summed up in table.2

Table 2. Thermodynamic parameters for SO_2 adsorption on ZnO–PVA nanocomposite.

Parameter	Value	Meaning
ΔH°	+38.92 kJ/mol	Endothermic process (adsorption improves with temp)
ΔS°	+77.98 J/mol·K	Increased randomness at the solid–gas interface
ΔG° (298 K)	+15.69 kJ/mol	Non-spontaneous under standard state
ΔG° (308–318)	~+14–15 kJ/mol	Becomes slightly more favorable with increasing T

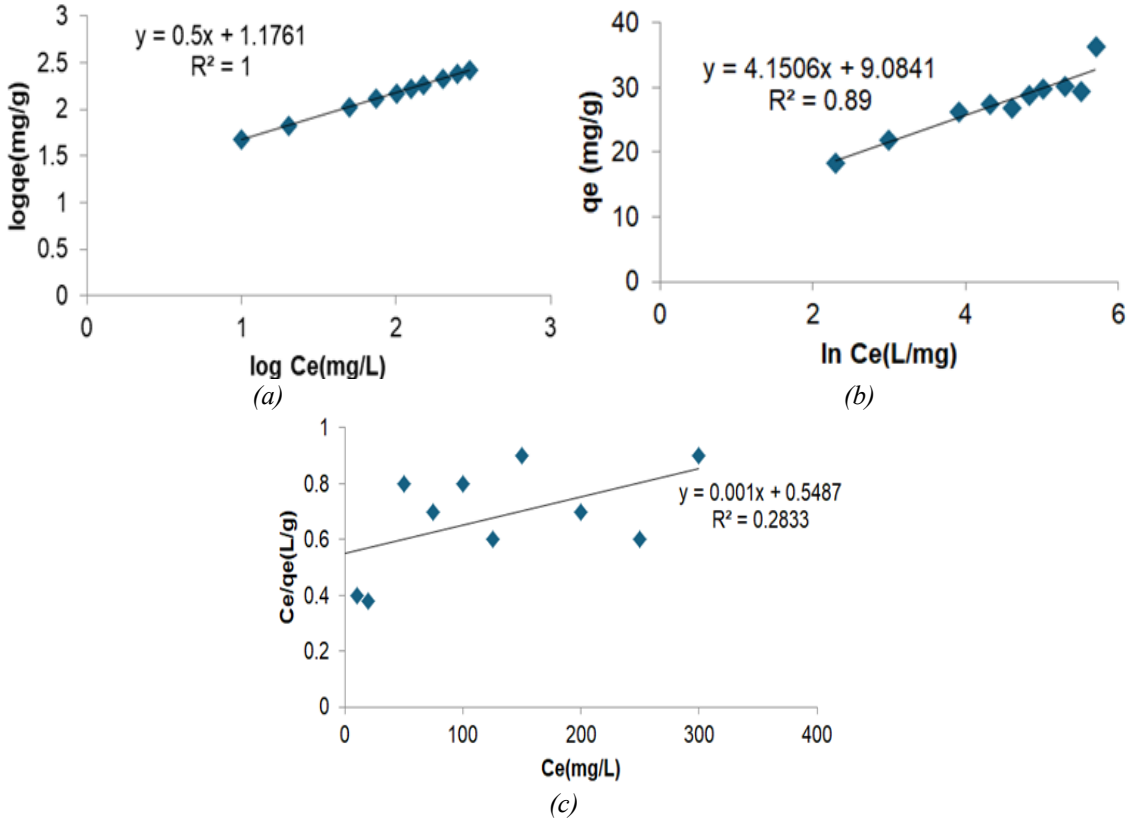

Fig. 11. (a), (b), (c) Freundlich, Temkin, and Langmuir isotherm plots for SO_2 adsorption on ZnO–PVA.

4. Conclusion

This work establishes the efficacy of ZnO–PVA nanocomposite as a viable material for SO_2 removal in bag house filter. Key findings include:

Enhanced SO_2 Adsorption: The ZnO–PVA composite has high adsorption capacity, governed by multilayer physisorption on heterogeneous surfaces, as indicated by the Freundlich model (R^2 = 1, 1/n =0.5 and KF =1.17).

Thermal and Chemical Stability: Thermal analysis confirmed that the material remains stable up to ~450 °C, retaining ~20% ZnO residue post-degradation essential for applications in high-temperature flue gas streams.

- Mechanistic Insights: FTIR and UV–Vis analyses confirmed the interaction between Zn^{2+} coordination sites and SO_2 molecules, suggesting a combination of reversible physical adsorption.

Structural Integrity: SEM and EDAX analyses post exposure showed no morphological deterioration or agglomeration, validating mechanical durability and uniformity of the nanocomposite under acidic conditions.

Sensor Potential: Optical stability studies and UV–Vis spectral shifts offer promise for the material's application in real-time SO_2 monitoring systems.

Thermodynamic Analysis ($\Delta H^\circ \approx +38.92$ kJ/mol $\Delta S^\circ \approx +77.98$ J/mol·K $\Delta G^\circ \approx +14$ kJ/mol) confirms that SO_2 adsorption on the ZnO–PVA nanocomposite is endothermic and entropy favored, indicating a physisorption mechanism.

Thus, this research confirms that ZnO–PVA is a suitable material for SO_2 removal in baghouse filters, effectively addressing a previously existing limitation. Further investigations into cyclic adsorption-desorption performance, long-term exposure stability and pilot-scale deployment are planned as future work.

References

[1] Yangxian Liu, Qian Wang, Jianfeng Pan, Environmental Science & Technology 50(23), 12966(2016); https://doi.org/10.1021/acs.est.6b02753

[2] Xiaojiao Chen, Xiaomin Hu, Energy & Fuels 33(7), 6707(2019); https://doi.org/10.1021/acs.energyfuels.9b00881

[3] L. Philip, M.A. Deshusses, Environmental Science & Technology, 37(9), 1978(2003); https://doi.org/10.1021/es026009d

[4] M.A. Hanif, N. Ibrahim, A. Abdul Jalil, Environmental Science and Pollution Research, 27(22), 27515(2020); https://doi.org/10.1007/s11356-020-09191-4

[5] P. Xie, C.L. Li, B. Shao, X.J. Xu, X.D. Chen, L. Zhao, X. Zhou, D.J. Lee, N.Q. Ren, C. Chen, Chemosphere, 276, 130084(2021); https://doi.org/10.1016/j.chemosphere.2021.130084

[6] H.S. Park, D. Kang, J.H. Kang, K. Kim, J. Kim, H. Song, International Journal of Environmental Research and Public Health, 18(2), 597(2021); https://doi.org/10.3390/ijerph18020597

[7] Jianliang Sun, Lianghai Li, Guangying Zhou, Xue Wang, Liang Zhang, Yueping Liu, Jierui Yang, Xianghong Lü, Feng Jiang, Environmental Science & Technology 52(8), 4754(2018), https://doi.org/10.1021/acs.est.7b06551

[8] Q. Zhang, T. Higuchi, M. Sekine, T. Imai, Environmental Technology, 30(14), 1529(2009); https://doi.org/10.1080/09593330903246440

[9] M.B. Chang, H.M. Lee, F. Wu, C.R. Lai, Journal of the Air & Waste Management Association, 54(8), 941(2004); https://doi.org/10.1080/10473289.2004.10470965

[10] C.H. Nelli, G.T. Rochelle, Journal of the Air & Waste Management Association, 48(9), 819(1998); https://doi.org/10.1080/10473289.1998.10463728

[11] I. Omidi Bibalani, H. Ale Ebrahim, Environmental Science and Pollution Research, 29(4), 6334(2022); https://doi.org/10.1007/s11356-021-16073-w

[12] H. Yu, C. Shan, J. Li, X. Hou, L. Yang, Journal of Environmental Management, 366, 121532(2024); https://doi.org/10.1016/j.jenvman.2024.121532

[13] J. Wei, J. Gu, J. Guo, W. Li, C. Wang, J. Zhang, Environmental Science and Pollution Research, 26(22), 22351(2019); https://doi.org/10.1007/s11356-019-05531-1

[14] C. Sun, J. Yuan, H. Xu, S. Huang, X. Wen, N. Tong, Y. Zhang, Bioresource Technology, 290, 121768(2019); https://doi.org/10.1016/j.biortech.2019.121768

[15] Ma Y, Qu Z, Xu H, Wang W, Yan N.J Hazard Mater, 279, 289(2014); https://doi.org/10.1016/j.jhazmat.2014.07.012

[16] D.S. Jin, B.R. Deshwal, Y.S. Park, H.K. Lee, Journal of Hazardous Materials, 135(1–3), 412(2006); https://doi.org/10.1016/j.jhazmat.2005.12.001

[17] L.C. Wu, T.H. Chang, Y.C. Chung, Journal of the Air & Waste Management Association, 57(12), 1461(2007); https://doi.org/10.3155/1047-3289.57.12.1461

[18] X.J. Xu, Y.N. Wu, Q.Y. Xiao, P. Xie, N.Q. Ren, Y.X. Yuan, D.J. Lee, C. Chen, Environmental Research, 205, 112541(2022); https://doi.org/10.1016/j.envres.2021.112541

[19] Yangxian Liu, Lei Liu, Yan Wang. Environmental Science & Technology , 55(14) , 9691(2021); https://doi.org/10.1021/acs.est.1c01531

[20] Yan Wang, Yong Wang, Yangxian Liu. Absorption of H2S from Gas Streams by the Wet Ultraviolet/Persulfate Oxidation Process: Mechanism and Kinetics. Energy & Fuels, 34(7), 8037(2020); https://doi.org/10.1021/acs.energyfuels.0c00755

[21] Hongyuan Xi, Song Zhou, Zhao Zhang, Energy & Fuels, 34(2), 1984(2020); https://doi.org/10.1021/acs.energyfuels.9b03617

[22] Juzheng Song, Liangliang Zhu, Xiaoyang Shi, Yilun Liu, Hang Xiao, Xi Chen, Energy & Fuels, 33(11), 10953(2019); https://doi.org/10.1021/acs.energyfuels.9b03297